Introducing Cu(II) onto SiO_2-TiO_2 with Rice Husk Ash as the Source of Silica and Its Catalytic Activity for Kumada Cross-coupling Reaction to Produce Biphenyl Compound

Dewi Agustiningsih[1], Nuryono Nuryono[2], Sri Juari Santosa[2], and Eko Sri Kunarti[2*]

[1]*Division of Inorganic and Physical Chemistry, Faculty of Mathematics and Natural Sciences, Institut Teknologi Bandung, Jl. Ganesha No. 10, Bandung 40132, Indonesia*

[2]*Department of Chemistry, Faculty of Mathematics and Natural Sciences, Universitas Gadjah Mada, Sekip Utara, Yogyakarta 55281, Indonesia*

** Corresponding author:*

tel: +62-81578634638
email: eko_kunarti@ugm.ac.id

Received: August 20, 2024
Accepted: April 8, 2025

DOI: 10.22146/ijc.99296

Abstract: *This research studied the preparation of SiO_2-TiO_2/Cu(II) by utilizing rice husk ash as the SiO_2 precursor, and evaluated its efficiency as a heterogeneous catalyst in biphenyl synthesis through Kumada cross-coupling reaction, which is widely known as an important intermediate in pharmacology and agriculture manufacturing. In this study, the catalyst preparation was conducted by extracting SiO_2 from rice husk ash, combining it with TiO_2, and introducing Cu(II) onto its surface with $CuCl_2{\cdot}2H_2O$ as the precursor with various concentration of Cu(II). Comprehensive characterization using techniques such as IR, XRD, XRF, DLS, N_2 isotherm adsorption-desorption, ICP-AES, STEM-EDS, TEM, and TGA was conducted to examine the catalyst properties. Catalyst activity was evaluated in the Kumada cross-coupling reaction, using phenylmagnesium bromide and bromobenzene as reactants under stirring-heating condition, and the products were analyzed using GC-FID method. The characterization results indicated that the preparation of SiO_2-TiO_2/Cu(II) materials was successfully conducted and Cu(II) was formed as $Cu(OH)_2$. The catalyst considerably promoted the Kumada cross-coupling reaction with a biphenyl yield of 78.85% at 50 °C for 6 h under stirring-heating method. Furthermore, catalyst reusability test demonstrated that the catalyst sustained performance over three cycles without losing its activity significantly. Interestingly, SiO_2-TiO_2 was observed to function primarily as support material and adsorbent, immobilizing Cu(II) and enhancing reactant reduction but not directly influencing biphenyl formation. Overall, this study contributes to the understanding of SiO_2-TiO_2/Cu(II) catalyst preparation and its application in biphenyl synthesis, offering insights into catalyst design and performance optimization for future applications in organic synthesis.*

Keywords: *biphenyl; copper; Kumada cross-coupling; rice husk ash; SiO_2-TiO_2*

■ INTRODUCTION

The synthesis of biphenyl and its application as an important intermediate in the development and design of high-affinity drugs has garnered significant interest among many chemists. This compound is extensively utilized in both academic and industrial research to produce pharmaceuticals, including highly active antihypertensive and anticancer agents [1]. In addition, it is often used in the development of functional materials and natural products [2]. A widely used method for synthesizing biphenyl is the Kumada carbon-carbon cross-coupling reaction, which typically involves homogeneous catalysts such as M(II)-phosphine complexes, where M can be metals like Pd, Co, Cu, Fe, and Ni [3-4]. The application of homogeneous catalysts in this reaction presents several challenges, such as difficulties in catalyst separation from the reaction mixture, limited reusability, and the potential for contaminating the final product. These issues are particularly problematic in the context of pharmacological synthesis [4-7].

To overcome the drawbacks of homogeneous catalysts, this study proposed the use of heterogeneous catalysts by dispersing active metal ions on solid support materials. This method allows for straightforward separation of the catalyst from the reaction products. Specifically, we used Cu(II) ions as the catalytically active species, dispersed on a mesoporous silica-titania (SiO_2-TiO_2) composite support. The selection of Cu(II) is based on its demonstrated efficiency in promoting the Kumada cross-coupling reaction, as highlighted in some previous research [8-11]. In this study, SiO_2 was selected as a primary support material due to its numerous benefits, such as the ability to form a great framework, its abundance in nature and living organisms, high surface area, significant thermal stability, and robust mechanical strength [12]. SiO_2 used in this research was derived from the extraction of rice husk ash, which is known to contain SiO_2 with high purity levels, ranging from 90 to 99% [13-17].

SiO_2, despite its widespread use as a support material for metals or metal ions, has a significant limitation, it exhibits poor compatibility with transition metals or metal ions which leads to weak interactions. As a result, the dispersion of transition metals or metal ions on the SiO_2 surface tends to be suboptimal [12]. A promising approach to addressing the inherent weaknesses of SiO_2 is to combine it with other support materials, such as TiO_2. TiO_2 possesses several beneficial properties that enhance and complement the capabilities of SiO_2 as a support material. Importantly, TiO_2 can form strong interactions with a variety of transition metals or metal ions, including gold, copper, nickel, manganese, palladium, cobalt, and ruthenium [18]. In composite systems, achieving optimal TiO_2-metal interaction can enhance the SiO_2-metal interaction. However, TiO_2 also faces several challenges, including low surface area, limited thermal stability, reduced adsorption capacity, and high tendency to agglomerate [19-20]. Therefore, combining SiO_2 and TiO_2 to become a composite is expected to result in a support material with high thermal stability, great surface area, and excellent ability to interact optimally with the metal or metal ion catalyst on its surface [21-22].

Previous studies have reported the use of SiO_2 and TiO_2 as support materials for dispersing metal or metal ion catalysts in cross-coupling reactions for biphenyl synthesis, as listed in Table 1. Among the catalysts examined, Ni and Pd metals or metal ions are the most

Table 1. The use of SiO_2 and TiO_2 as support materials of heterogeneous catalyst in cross-coupling reactions for biphenyl synthesis

Catalyst	Reaction	Ref.
$NiFe_2O_4$@SiO_2-BPMN-Ni	Kumada	[23]
Pd-(EDTA)-coated Fe_3O_4@SiO_2	Suzuki and Sonogashira	[24]
Fe_3O_4@SiO_2@NHC@Pd	Suzuki-Miyaura	[25]
Pd/SiO_2	Suzuki-Miyaura	[26]
Fe_3O_4@SiO_2@NHC^SPh-Pd(II)	Sonogashira and Stille	[27]
Fe_3O_4@SiO_2-TCT-GA-Pd(0)	Suzuki-Miyaura	[28]
Pd(II-0)@m-SiO_2	Suzuki	[29]
Fe_3O_4@SiO_2/GO–NH_2–Co(II)	Mizoroki-Heck	[30]
Fe_3O_4@SiO_2@4-ABPT/Cu–Ni	Sonogashira	[31]
BisPyP@bilayer-SiO_2@NMP	Suzuki and Stille	[32]
Cu@Fe_3O_4-TiO_2-L-dopa	Chan-Lam	[33]
Pd(II)[PTATAD]@TiO_2	Sonogashira	[34]
TiO_2-AA-Pd	Suzuki-Miyaura	[35]
Ag/TiO_2	Suzuki	[36]
CuL@TiO_2@Fe_3O_4	Buchwald-Hartwig	[37]
$NiFe_2O_4$@TiO_2-Pd	Sonogashira	[38]
Ni/TiO_2	Suzuki-Miyaura	[39]
TiO_2@BDP-$PdCl_2$	Suzuki-Miyaura	[40]

frequently used, while Cu has been comparatively underutilized as catalysts in cross-coupling reactions for biphenyl synthesis. In this study, SiO_2-TiO_2 composite was designed to have mesoporous properties with pore sizes ranging from 2 to 50 nm. The reason for designing mesoporous composite in this case is because mesoporous materials have many advantages including their unique framework feature, large surface area, uniform pore size and shape, large pore volume, and ease of functionalization [41].

EXPERIMENTAL SECTION

Materials

The materials used in this study were chemicals with pro-analysis quality purchased from Sigma-Aldrich, Merck, TCI Chemicals, and Wako including HCl 37%, NaOH, $Ti(OCH(CH_3)_2)_4$ 97%, C_2H_5OH 99%, $C_{19}H_{42}BrN$ 98%, $CuCl_2{\cdot}2H_2O$ 99.9%, C_4H_8O deoxygenated 99.5%, C_6H_5MgBr 16% in THF, C_6H_5Br 98%, and $C_{14}H_{30}$ 99%. Other technical-grade chemicals were also used including Milli-Q water and rice husk ash (RHA) obtained from Yogyakarta, Indonesia. No additional purification was conducted for all the chemicals used.

Instrumentation

The instrumentations used for materials characterization in this research included X-ray fluorescence (XRF, NEXQC$^+$, QUANTEZ), attenuated total reflectance-infrared spectroscopy (ATR-IR, NICOLET iS10 PIKE GladiATR, Thermo Scientific), powder X-ray diffractometer (XRD, D2 PHASER 2nd Generation, Bruker), scanning transmission electron microscope-energy dispersive X-ray spectroscopy (STEM-EDS, HD-2000, HITACHI), thermogravimetric analyzer (TGA, Thermo plus TG 8120, Rigaku), N_2 isotherm adsorption-desorption analyzer (BELSORP-mini II, Microtrac), transmission electron microscope (TEM, JEM-2010, JEOL), dynamic light scattering (DLS, Zetasizer Pro, Malvern), and inductively coupled plasma-atomic emission spectroscopy (ICP-AES, ICPE-9000, Shimadzu).

Procedure

Preparation of mesoporous SiO_2-TiO_2 composite

The experimental procedure was started by washing rice husk (RH) and then combusting it in an open space. Next, the obtained RHA from the first combustion was leached by dispersing it in 1 M HCl with a ratio of 1:10 (m/v), stirring the mixture at room temperature for 2 h, and washing it with Milli-Q water. The leached RHA was then dried at 80 °C for 8 h before undergoing calcination at 550 °C for 5 h (analyzed using XRF). To extract silica, the calcined RHA was dispersed in 1 M NaOH with a ratio of 1:10 (m/v) and was stirred at 90 °C for 2 h, after which centrifugation at 4,000 rpm for 20 min was conducted to collect sodium silicate liquid as the SiO_2 precursor. The preparation of mesoporous SiO_2-TiO_2 composite was then carried out by neutralizing the obtained sodium silicate with 1 M HCl. Subsequently, titanium(IV) tetraisopropoxide (TTIP) precursor, dispersed in absolute ethanol with a ratio of 1:10 (m/v), was incorporated into the SiO_2 sol formed previously using a sonication system for 15 min. Cetyltrimethylammonium bromide (CTAB) as a template was then dissolved in 0.5 M aqueous NH_3 1:10 (v/v). After the complete dissolution of CTAB, SiO_2-TiO_2 sol was added to the CTAB solution with a molar ratio between each component of SiO_2:TiO_2:CTAB of 1:1:1 mol ratio. The mixture of SiO_2, TiO_2, and CTAB was stirred at room temperature for 6 h to produce a solid white gel. The gel was allowed to stand at room temperature for 12 h, collected by filtration, washed with Milli-Q water, and dried at 60 °C for 24 h. The template was then removed by conducting calcination at 600 °C for 3 h in air flow (10 mL min^{-1}).

Introduction of Cu(II) onto SiO_2-TiO_2 surface

Mesoporous SiO_2-TiO_2 composite (1 g) was dispersed into Milli-Q water with a ratio of 1:10 (m/v). Simultaneously, Cu(II) solution was made by dissolving $CuCl_2{\cdot}6H_2O$ in various concentrations (3, 5, 7, and 10 mmol). The prepared Cu(II) solution was then added to SiO_2-TiO_2 suspension, and the mixture was stirred at room temperature for 24 h. The obtained solid material was filtered, washed three times with Milli-Q water, and dried at 60 °C for 24 h. The catalyst materials were then comprehensively characterized using ATR-IR, XRD, STEM-EDS, TEM, TGA, N_2 isotherm adsorption-desorption analyzer, DLS, and ICP-AES.

Catalytic activity evaluation

The Kumada cross-coupling reaction was conducted as follows: phenylmagnesium bromide (1 mmol), bromobenzene (1 mmol), and 2 mL of deoxygenated tetrahydrofuran were added in a reaction tube. Additionally, 0.5 g of the catalyst material was added to the mixture. The reaction was performed under various reaction temperature (40, 50, 60, 70, and 80 °C) and time (1, 3, 6, and 9 h), using stirring and heating method. Upon completion of the reaction, the solid catalyst was separated by filtration with a syringe filter (pore size of 0.1 µm). The resulting products were subjected to analysis using gas chromatography with flame ionization detection (GC-FID), using a DB-17 column, with tetradecane serving as the internal standard. The Eq. (1) was used to determine the biphenyl yield percentage;

$$\text{Yield} = \frac{\text{mmol of produced biphenyl}}{1\ \text{mmol}} \times 100\% \quad (1)$$

To quantify the moles of biphenyl produced, we prepared a series of standard solutions. Each solution contained various amounts of biphenyl (0, 0.25, 0.50, 0.75, and 1.0 mmol) and a fixed amount of tetradecane (0.4 mmol), diluted to a total volume of 10 mL with THF. The standard solutions were analyzed using GC-FID, generating chromatograms with peak area data for both biphenyl and tetradecane. We calculated the biphenyl/tetradecane molar ratio for each solution and plotted it against the corresponding peak area ratio. This allowed us to derive a linear equation. This equation was then used in the GC-FID analysis of the liquid products from the catalytic reaction. By determining the peak area ratio in the product chromatogram, we could calculate the molar ratio of biphenyl/tetradecane and thus quantify the moles of biphenyl produced.

Biphenyl isolation

The isolation process was initiated by collecting the crude liquid produced, which was washed with a 5 mL mixture of Milli-Q water and ethyl acetate in a 1:2 (v/v) ratio. This procedure resulted in the formation of two different layers: an upper organic layer and a lower aqueous layer. The aqueous layer was washed three additional times with 5 mL of pure ethyl acetate. All organic layers were combined and dried over anhydrous Na_2SO_4. The dried organic phase was further purified by evaporating the solvent using a rotary evaporator at 90 °C for 30 min. After completion of the evaporation, a small amount of white crystals, identified as 1,1'-biphenyl, was obtained. These crystals were characterized using attenuated total reflectance-infrared spectroscopy (ATR-IR), proton nuclear magnetic resonance (^{1}H-NMR), carbon nuclear magnetic resonance (^{13}C-NMR), CHNS analysis, melting point determination, and thin-layer chromatography (TLC).

■ RESULTS AND DISCUSSION

Catalyst Materials Characterization

The extraction of silica from RH was initiated by washing the husks using Milli-Q water to obtain clean RHA (Fig. 1(a)). These cleaned husks were then burned in an open space, producing black RHA. This initial combustion aimed to remove carbon components before

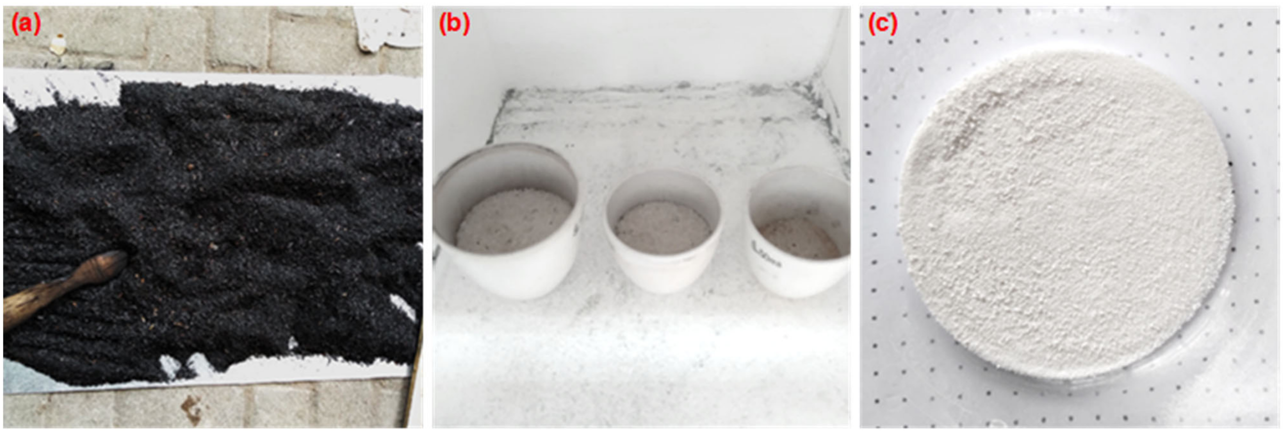

Fig 1. (a) Leached RHA, (b) calcined RHA, and (c) extracted SiO_2

subsequent high-temperature calcination. Once the black RHA obtained from the first combustion, it was then dispersed into a 1 M HCl solution at a ratio of 1:10 (w/v). This acid leaching process helped eliminate alkali metals such as calcium, sodium, and magnesium, as well as other transition metal oxides present in the ash. The reduction of these metal components in the ash increased the relative SiO_2 content, achieving a purity of over 90%. As shown in Table 2, after the initial combustion and HCl treatment, the RHA contained a higher SiO_2 content (6.91%) compared to other metal oxides, although the carbon content remained high due to the moderate initial combustion temperature. The subsequent step involved calcining the RHA produced from the previous steps, including the first burning and HCl washing (acid leaching). The calcination aimed to further remove carbon components from the ash, resulting in high-purity SiO_2, indicated by the color change from black to white (Fig. 1(b)). Table 2 also demonstrates the increase in SiO_2 content and the decrease in carbon content after calcination, indicating that most of the carbon had been successfully burned to CO_2, thus relatively increasing the SiO_2 content. In this study, calcination was performed at 550 °C for 5 h. Naturally, SiO_2 exists in an amorphous phase, but this structure can transform into a crystalline form depending on the thermal conditions during extraction. The transformation from amorphous to crystalline SiO_2 with increasing temperature will reduce silanol functional groups on the surface necessary for subsequent modification. Therefore, to maintain the amorphous structure, calcination was conducted at 550 °C for 5 h. Lower temperatures (300–450 °C) were not used because they could result in incomplete carbon combustion [42-43], producing coke that would reduce the purity and surface area of the SiO_2. The final step in silica extraction from calcined RHA was dispersing the white ash in a 1 M NaOH solution at a ratio of 1:10 (w/v). The mixture was stirred at 90 °C for 2 h, and the resulting sodium silicate supernatant was neutralized with 1 M HCl until pH 7 was reached. At neutral pH, silica gel was formed, allowed to stand for 24 g, washed with Milli-Q water, and dried at 60 °C for 12 h to yield white SiO_2 solid, as shown in Fig. 1(c). The chemical reactions involved in these processes are presented in Eq. (2) and (3) [44-47];

Table 2. XRF analysis result of extracted RHA

Component	Mass (%)	
	Before calcination	After calcination
SiO_2	8.64	98.72
Fe_2O_3	0.16	0.24
C	90.75	0.14
K_2O	0.27	0.48
CaO	0.10	0.26
TiO_2	0.08	0.16

$$SiO_{2(s)}(RHA) + 2NaOH_{(aq)} \rightarrow Na_2SiO_{3(aq)} + H_2O_{(l)} \quad (2)$$

$$Na_2SiO_{3(aq)} + 2HCl_{(aq)} \rightarrow SiO_{2(s)}(gel) + 2NaCl_{(aq)} + H_2O_{(l)} \quad (3)$$

The study continued with the preparation of SiO_2-TiO_2 composites using CTAB as a surfactant and the immobilization of Cu(II) ions on the composite surface with $CuCl_2·2H_2O$ as the precursor. CTAB was chosen for its strong capability to prevent agglomeration of SiO_2-TiO_2 particles and its cost-effectiveness [48]. After the preparation process, the materials were characterized using ATR-IR, and XRD, TGA. In the IR spectra of SiO_2-TiO_2 and SiO_2-TiO_2/Cu(II) composites (Fig. 2(a)), the SiO_2-TiO_2 composite showed characteristic vibration bands including O–H stretching at 3000–3500 cm^{-1}, O–H bending at 1635 cm^{-1}, Si–O–Si bending or O–Ti–O stretching at 462 cm^{-1} [49-51], symmetric stretching of Si–O–Si at 790 cm^{-1}, asymmetric stretching of Si–O–Ti at 945 cm^{-1}, and asymmetric stretching of Si–O–Si at 1075 cm^{-1}. There were no significant changes in the spectra of SiO_2-TiO_2 after Cu(II) immobilization, indicating that Cu(II) was likely dispersed on the external surface of the composite, thus not altering the main SiO_2-TiO_2 framework and its internal bonds.

The diffraction pattern presented in Fig. 2(b) reveals that SiO_2-TiO_2 composite showed amorphous properties inherent to the composite phase. It is known that TiO_2 typically forms a crystalline anatase phase at room temperature [52-54], however, this did not occur in our study. This suggests that the presence of SiO_2 as a matrix in SiO_2-TiO_2 composite may inhibit the crystallization of TiO_2 which implies that TiO_2 was highly dispersed within the SiO_2 framework [55]. However, upon the immobilization of Cu(II) ions onto

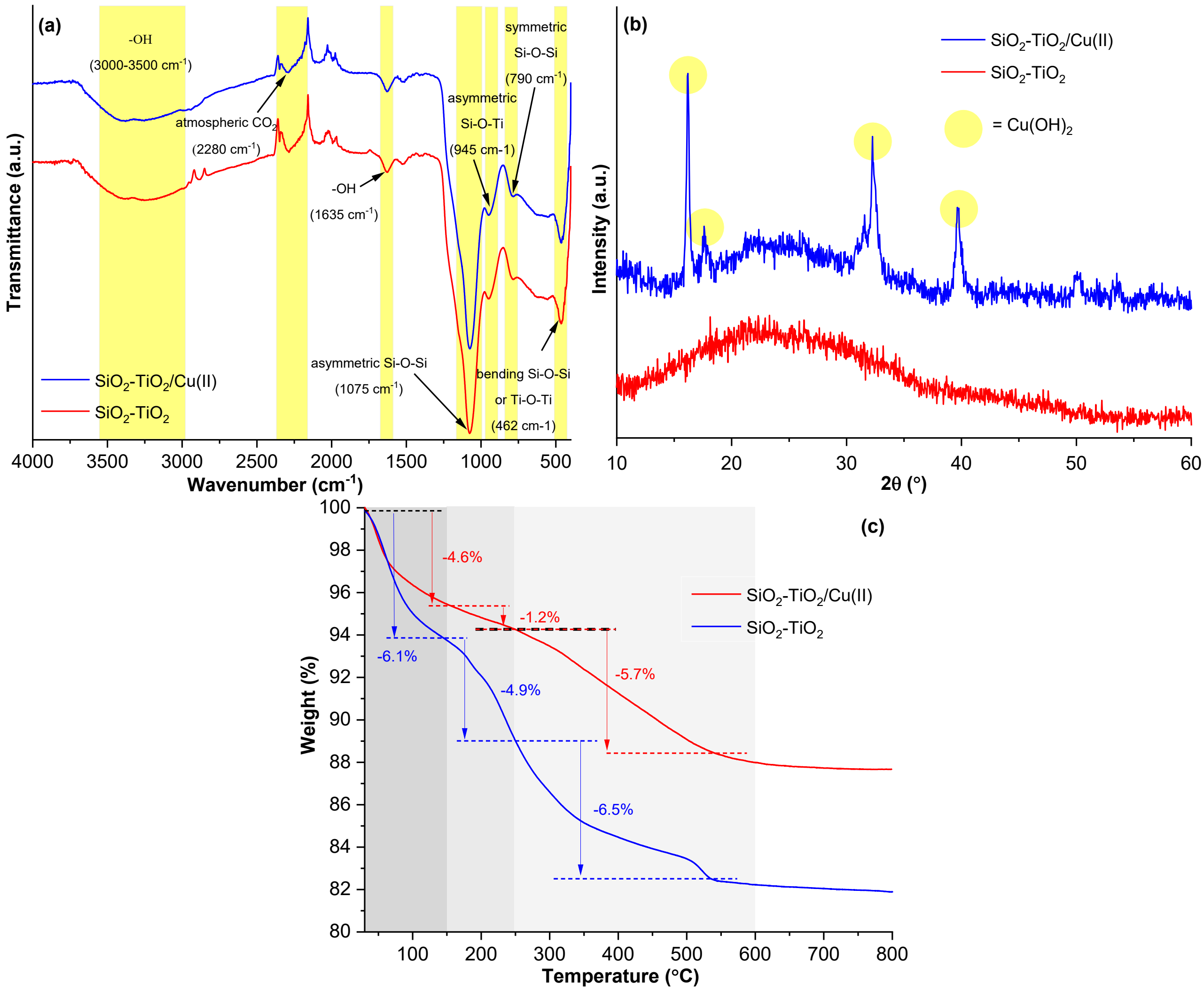

Fig 2. (a) IR spectra, (b) diffraction pattern, and (c) TG curve of SiO_2-TiO_2 and SiO_2-TiO_2/Cu(II)

SiO_2-TiO_2 surface, new diffraction peaks were observed. These peaks at 2θ values of 16, 18, 32, and 38° (JCPDS No. 13-420) correspond to bulk $Cu(OH)_2$ [56-57]. The formation of $Cu(OH)_2$ on SiO_2-TiO_2 surface was related to the solubility product (K_{sp}) of the hydroxide compound. $Cu(OH)_2$ has a K_{sp} of 2.2×10^{-20} at 25 °C which indicates that Cu(II) ions precipitate easily. To further understand the behavior of hydroxide formation in Cu(II) metal ion, an experiment was conducted where the pH of a $CuCl_2{\cdot}2H_2O$ solution was adjusted using $NaOH_{(aq)}$, and the changes in the solution appearance were monitored. The initial pH of the $CuCl_2{\cdot}2H_2O$ solution was 3.2, and the solution was observed to be clear blue (Fig. 3). Upon the gradual addition of $NaOH_{(aq)}$, hydroxide formation was noted when the pH reached 3.5.

Fig 3. $Cu(OH)_2$ formation in $CuCl_2{\cdot}2H_2O$ solution after the addition of NaOH at pH of 3.2 (left) and 3.5 (right)

This indicates that $Cu(OH)_2$ precipitates readily, even at relatively low pH levels. Furthermore, the basic hydroxyl groups present on SiO_2-TiO_2 surface caused an increase in the pH of the $CuCl_2 \cdot 6H_2O$ solution when SiO_2-TiO_2 was added. Thus, Cu(II) was precipitated and $Cu(OH)_2$ was formed.

Thermal profile and mass reduction data as a function of temperature for SiO_2-TiO_2 and SiO_2-TiO_2/Cu(II) materials, as illustrated in Fig. 2(c), reveal three distinct thermal phenomena for SiO_2-TiO_2. Firstly, physically adsorbed water molecules were released from SiO_2-TiO_2 surface within the temperature range of 30–150 °C. Secondly, between 150–250 °C, chemically adsorbed water molecules within SiO_2-TiO_2 framework and water molecules resulting from the condensation of silanol and titanol groups were released. Lastly, the combustion of residual organic components from CTAB occurred in the temperature range of 250–600 °C after the template removal process. For SiO_2-TiO_2/Cu(II) material, a reduction in the number of physically adsorbed water molecules on the composite surface was observed, indicating that the presence of $Cu(OH)_2$ on the surface inhibited interaction with water molecules, thereby reducing water adsorption. Furthermore, there was a decrease in the amount of residual organic CTAB after calcination, which was likely due to the partial dissolution of CTAB during the Cu(II) immobilization process.

Fig. 4 and 5 illustrate STEM images and elemental mapping of SiO_2-TiO_2 and SiO_2-TiO_2/Cu(II) materials, respectively. The particles of these materials generally exhibited a quasi-spherical shape. Initially, SiO_2-TiO_2 surface appeared to be quite rough, but it became smoother upon Cu(II) immobilization, likely due to the presence of $Cu(OH)_2$ precipitates covering the surface. Elemental mapping using EDS confirms the detection of constituent elements in both materials, including Si, Ti, O, and Cu, with uniform distribution observed across the particle surfaces. Fig. 6 illustrates TEM images of SiO_2-TiO_2 and SiO_2-TiO_2/Cu(II) materials. As depicted, SiO_2-TiO_2 showed quasi-spherical particle structures. Following Cu(II) immobilization, dark-colored particles were observed on SiO_2-TiO_2 surface, likely representing $Cu(OH)_2$ species covering the material entirely.

The N_2 adsorption-desorption isotherms and accompanying data, such as the BET surface area, total pore volume, and average pore diameter of both SiO_2-TiO_2 and SiO_2-TiO_2/Cu(II) materials, are presented in Fig. 7 and Table 3, respectively. As listed in Table 3, the immobilization of Cu(II) metal ions onto SiO_2-TiO_2

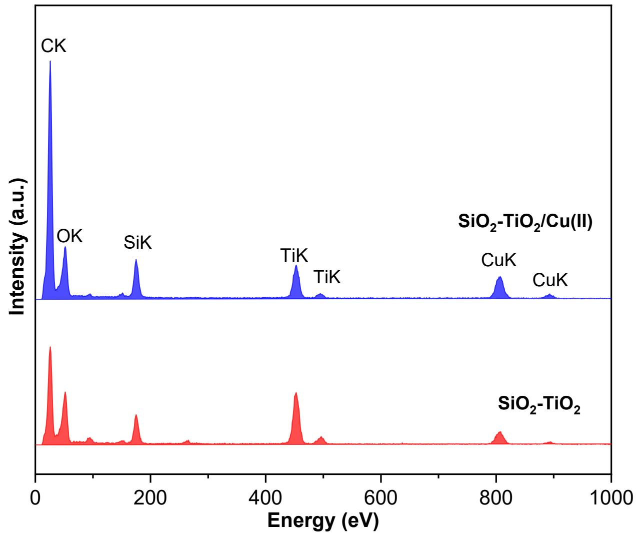

Fig 5. EDS spectra of (a) SiO_2-TiO_2 and (b) SiO_2-TiO_2/Cu(II)

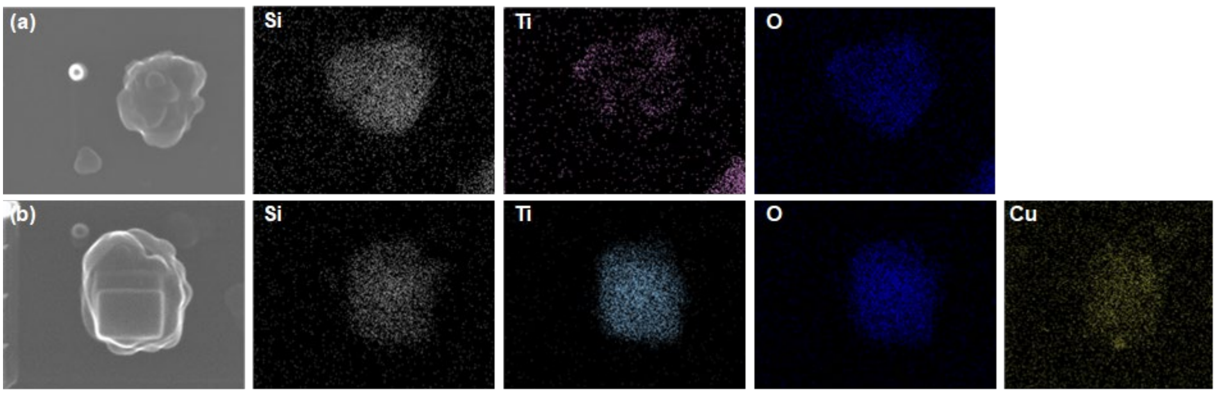

Fig 4. STEM images of (a) SiO_2-TiO_2 and (b) SiO_2-TiO_2/Cu(II)

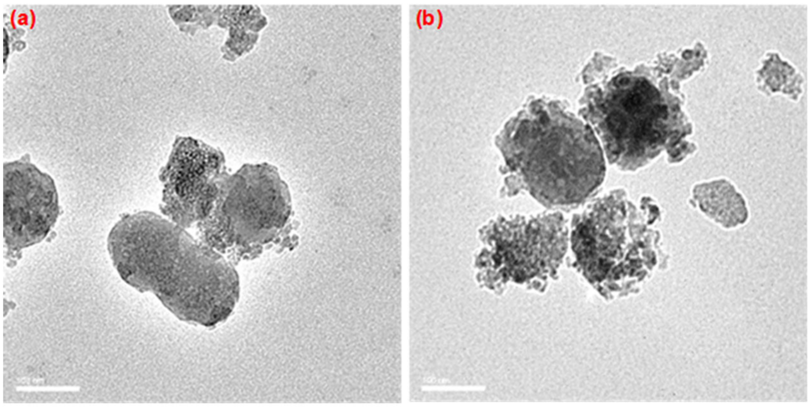

Fig 6. TEM images of (a) SiO_2-TiO_2 and (b) SiO_2-TiO_2/Cu(II)

surface led to a reduction in the BET surface area, total pore volume, and average pore diameter. This phenomenon can be attributed to the presence of Cu(II) ions as $Cu(OH)_2$ precipitates on SiO_2-TiO_2 surface, which effectively covered nearly all external and internal active sites and clogged the pore. In addition, the increase in Cu(II) dosage during the immobilization process caused bigger decline in those parameters as the pore surfaces became more covered and clogged. Furthermore, as illustrated in Fig. 7, N_2 adsorption-desorption isotherms of both samples exhibited hysteresis loop with type IV starting from $P/P_0 > 0.4$. This suggests that both materials had well mesoporous character. Fig. 8 and Table 4 show Cu^{2+} doses sequentially introduced during the preparation process of SiO_2-TiO_2 and SiO_2-TiO_2/Cu(II), along with the actual concentrations detected by ICP-AES instrument**.** Fig. 8 shows that the concentrations of metal ions and Cu^{2+} generally increase with dose increments, yet the actual concentrations consistently remain lower than the doses introduced during preparation. This indicates that only a portion of these metal ions successfully immobilize on SiO_2-TiO_2 surface, likely due to the limited number of oxygen atoms from O–H groups on composite surface which serve as binding sites.

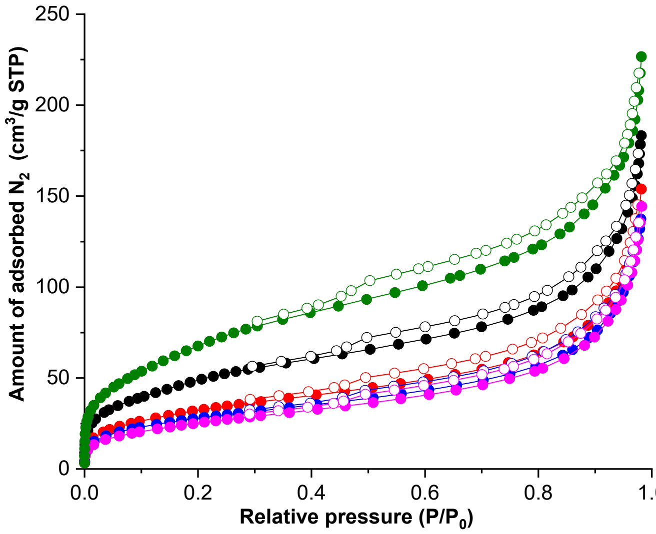

Fig 7. N_2 isotherm adsorption-desorption of SiO_2-TiO_2 (●,○), SiO_2-TiO_2/Cu(II) 3 mmol/g (●,○), 5 mmol/g (●,○), 7 mmol/g (●,○), and 10 mmol/g (●,○). Closed and opened symbols are adsorption and desorption plot, respectively

Table 3. N_2 isotherm adsorption-desorption data of the prepared materials

Material	BET surface area ($m^2\ g^{-1}$)	Pore total volume ($cm^3\ g^{-1}$)	Pore average diameter (nm)
SiO_2-TiO_2	236.43	0.35	15.93
SiO_2-TiO_2/Cu(II) 3 mmol/g	163.29	0.28	10.30
SiO_2-TiO_2/Cu(II) 5 mmol/g	108.22	0.24	9.09
SiO_2-TiO_2/Cu(II) 7 mmol/g	93.49	0.21	8.19
SiO_2-TiO_2/Cu(II) 10 mmol/g	86.69	0.22	7.00

Table 4. Dosage and actual amount of Cu(II) in each sample detected by ICP-AES

Material	Dosage (mmol/g)	Actual amount (mmol/g)
SiO_2-TiO_2/Cu(II) 3 mmol/g	3	4.20
SiO_2-TiO_2/Cu(II) 5 mmol/g	5	5.23
SiO_2-TiO_2/Cu(II) 7 mmol/g	7	4.82
SiO_2-TiO_2/Cu(II) 10 mmol/g	10	6.35

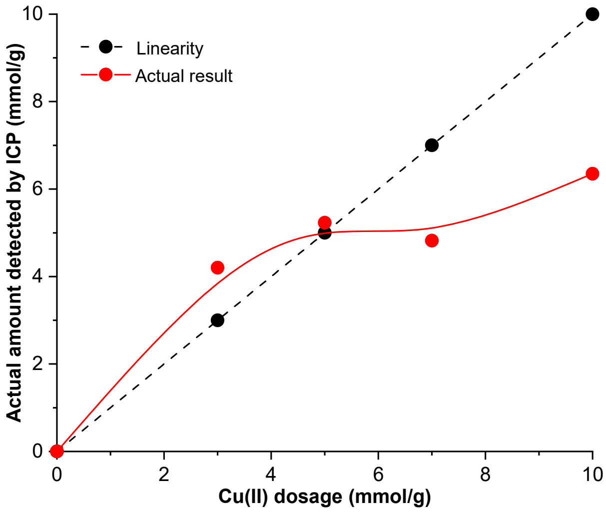

Fig 8. Dosage and actual amount of Cu(II) in each sample detected by ICP-AE

Fig. 9 depicts the particle size distribution of both SiO_2-TiO_2 and SiO_2-TiO_2/Cu(II). It is seen that the average particle size of SiO_2-TiO_2 composite is around 200 nm. CTAB made a crucial contribution in preventing agglomeration of SiO_2-TiO_2 particles during the preparation process. Initially, CTAB molecules underwent a self-assembly process to form micelles, in which the polar ends of CTAB molecules oriented outward to interact with water molecules, while the non-polar ends gathered internally. Subsequently, SiO_2-TiO_2 precursors continuously filled the internal spaces of these micelles through a mechanism known as co-assembly. In the template removal with calcination method, CTAB molecules were removed, leaving behind finely sized SiO_2-TiO_2 particles. Despite the addition of CTAB as a surfactant and capping agent to prevent agglomeration, the obtained particle size remained relatively large, falling outside the nano-dimension. This is due to the higher tendency for agglomeration of amorphous SiO_2 and TiO_2 compared to their crystalline phases, resulting in larger composite particle sizes [58-60]. Furthermore, the average particle size increased with the immobilization of Cu(II) on the SiO_2-TiO_2 composite surface. This is due to Cu(II) being immobilized as $Cu(OH)_2$ precipitates, which naturally have larger sizes. Increasing Cu(II) dosage also led to an increase in the average particle size, as more $Cu(OH)_2$ accumulated on the composite surface. Fig. 10 presents the zeta potential values of SiO_2-TiO_2 and SiO_2-TiO_2/Cu(II). SiO_2-TiO_2 exhibited a negative zeta potential originating from either silanol or titanol O–H groups on its surface which carried partial negative charges. In contrast, SiO_2-TiO_2/Cu(II) showed a more positive zeta potential compared to SiO_2-TiO_2, due to the natural positive charge of the immobilized Cu(II) ions. This zeta potential became increasingly positive with the concentration of Cu(II) metal ions.

Based on the characterization data and subsequent discussions, we propose the structures of SiO_2-TiO_2 and SiO_2-TiO_2/Cu(II), as shown in Fig. 11. Cu(II) was immobilized onto SiO_2-TiO_2 surface and was formed as $Cu(OH)_2$ precipitates, which likely interacted with the

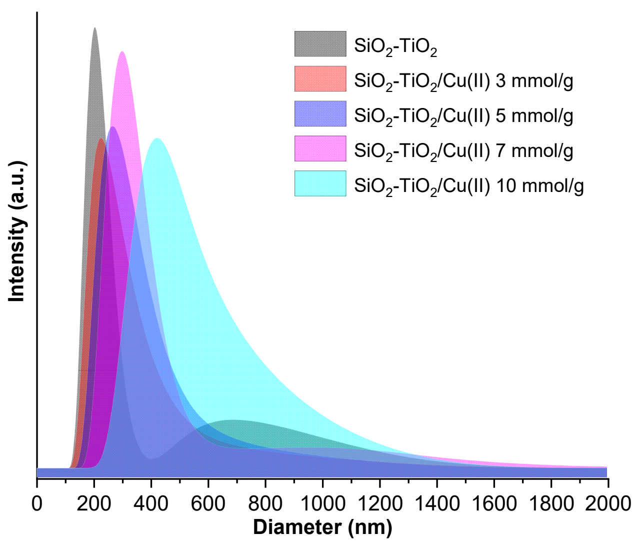

Fig 9. Particle size distribution of the prepared samples

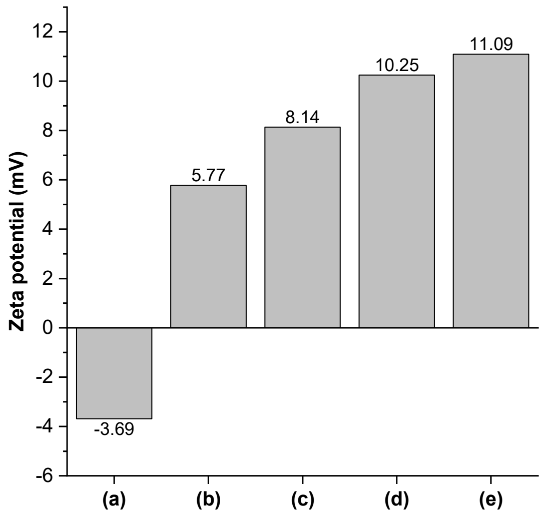

Fig 10. Zeta potential of the prepared samples (a) SiO_2-TiO_2 and SiO_2-TiO_2/Cu(II) (b) 3, (c) 5, (d) 7, and (e) 10 mmol/g

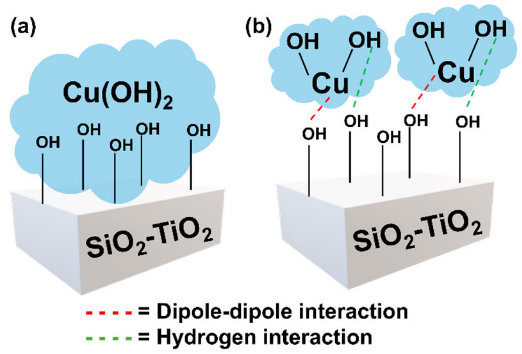

Fig 11. Plausible structure of (a) SiO_2-TiO_2/Cu(II), (b) interaction between SiO_2-TiO_2 and Cu(II) as $Cu(OH)_2$ on the surface

surface predominantly through dipole-dipole interactions between partially positive Cu(II) species and partially negative oxygen of O–H groups of SiO_2-TiO_2, as well as hydrogen interactions between O–H groups attached to Cu(II) species and O–H groups on composite surface.

Table 5 shows the optimization data of Kumada cross-coupling reaction under different temperatures. The data reveal that biphenyl yield increased alongside the increase in reaction temperatures, reaching an optimum at 50 °C. This increase in yield was due to the higher energy available at higher temperatures, which enhanced the Kumada cross-coupling reaction. Higher temperatures provided more thermal energy converted into kinetic energy, causing reactant molecules to move faster, and increasing the probability of collisions between them. However, catalytic activity began to decline when the reaction temperature exceeded 50 °C, due to the leaching probability of Cu(II) or $Cu(OH)_2$ serving as active site on the catalyst surface. Previous studies have also reported that high temperatures in cross-coupling reactions can lead to side reactions, destabilization of reactants, and degradation of products [61-63]. To support these observations, a Kumada cross-coupling reaction was conducted at 80 °C under the same conditions as before. After the reaction was completed, the catalyst was recovered, washed, dried, and reused in a reaction at 50 °C. The biphenyl yield in this second reaction was similar to that obtained at 80 °C, indicating that at the higher temperature of 80 °C, active metal species were leached from the catalyst surface, thus significantly reducing its catalytic activity. Based on the temperature optimization results, it was determined that the optimum temperature for the catalytic Kumada cross-coupling reaction in this study was 50 °C.

Fig. 12 displays the optimization data for the reaction time in the Kumada cross-coupling reaction under the specified conditions. The biphenyl yield showed a gradual increase up to 6 h (78.85%), after which

Table 5. Catalytic activity of SiO_2-TiO_2/Cu(II) with different Cu(II) dosages under different reaction temperatures

Catalyst	Yield of biphenyl (%) at temperature (°C)				
	40	50	60	70	80
SiO_2-TiO_2/Cu(II) 3 mmol/g	14.88	10.48	10.71	9.06	9.94
SiO_2-TiO_2/Cu(II) 5 mmol/g	20.67	24.01	17.55	11.11	8.73
SiO_2-TiO_2/Cu(II) 7 mmol/g	33.44	31.02	18.39	10.04	8.75
SiO_2-TiO_2/Cu(II) 10 mmol/g	39.20	39.43	26.16	12.30	7.38

Reaction condition: catalyst, 50 mg; reactants, PhMgBr and BrPh, 1 mmol for each; solvent, deoxygenated THF, 2 mL; time, 3 h; and method, stirring-heating

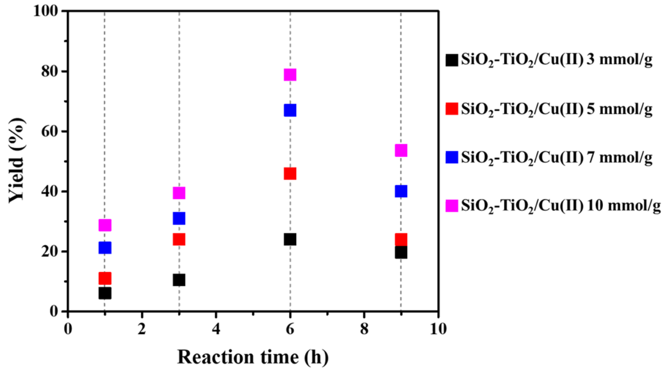

Fig 12. Catalytic activity of SiO_2-TiO_2/Cu(II) with different Cu(II) dosages at different reaction times. Reaction condition: catalyst, 50 mg; reactants, PhMgBr dan BrPh, 1 mmol for each; solvent, deoxygenated THF, 2 mL; temperature, 50 °C; and method, stirring-heating

it significantly decreased when the reaction time was extended to 9 h. This trend suggests that while longer reaction times initially allowed more reactants to participate in the reaction, excessive reaction time led to strong adsorption of the formed products on the catalyst surface. This strong adsorption likely hindered their release, resulting in a decreased biphenyl yield.

Fig. 13 shows the activity of various materials prepared in this study. SiO_2-TiO_2 as support material showed no catalytic activity in the Kumada cross-coupling reaction, as no biphenyl was produced. This lack of activity was due to the absence of catalytic active sites on the support material, specifically Cu(II) ions. The efficiency of SiO_2 and TiO_2 as support materials (with the same for Cu(II) was also evaluated, revealing that TiO_2/Cu(II) exhibited higher catalytic activity than SiO_2/Cu(II). As highlighted in the Introduction, SiO_2 has a lower ability to interact with metal ions compared to TiO_2, which resulted in fewer metal ions being dispersed on the surface of SiO_2 than on TiO_2 [12,18]. Interestingly, when SiO_2 and TiO_2 were combined, the catalytic activity increased, likely due to the synergistic interaction between SiO_2 and TiO_2. This synergistic effect enhanced the dispersion of metal ions on SiO_2-TiO_2 surface by increasing the number of surface O–H groups that interacted with the metal ions. Furthermore, SiO_2 may act as a dispersion matrix for TiO_2, preventing the agglomeration of TiO_2 particles and thereby increasing the surface area available for Cu(II) immobilization.

A reusability test was conducted for the SiO_2-TiO_2/Cu(II) catalyst under optimized conditions. After the reaction finished, the catalyst was filtered, washed sequentially with tetrahydrofuran, ethanol, and Milli-Q water (3 × 5 mL each), dried at 60 °C for 24 h, then reused for the next cycle. The results of the reusability test are presented in Fig. 14, showing a decrease in catalytic activity with each successive cycle. To investigate the reasons behind the decline in catalytic activity upon reuse, the spent catalyst after the third cycle was characterized using IR, XRD, and N_2 isotherm adsorption-desorption. These results were compared with those of the fresh catalyst, as shown in Fig. 15. The IR spectra and XRD patterns of the fresh and spent catalysts revealed no significant differences, indicating that catalyst main structure remained unchanged after repeated use in the Kumada cross-coupling reaction. However, N_2 isotherm adsorption-desorption data showed an increase in BET surface area from the fresh to the spent catalysts. This increase was likely due to the leaching of Cu(II) as $Cu(OH)_2$ from the catalyst surfaces,

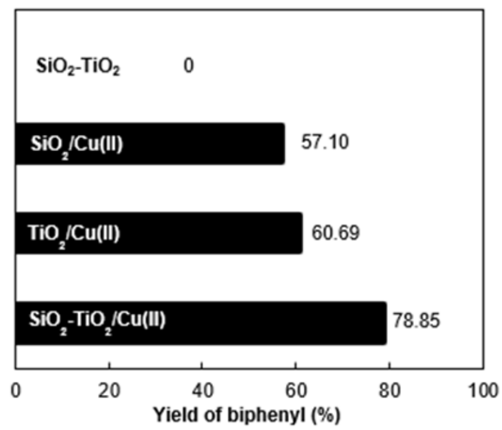

Fig 13. Catalytic activity comparison of the prepared materials. Reaction condition: catalyst, 50 mg; reactants, PhMgBr dan BrPh, 1 mmol for each; solvent, deoxygenated THF, 2 mL; time, 6 h; temperature, 50 °C; and method, stirring heating. The mol/mass ratios between Cu(II) and each support material were made the same, where 10 mmol of Cu(II) was immobilized in 1 g of each support material

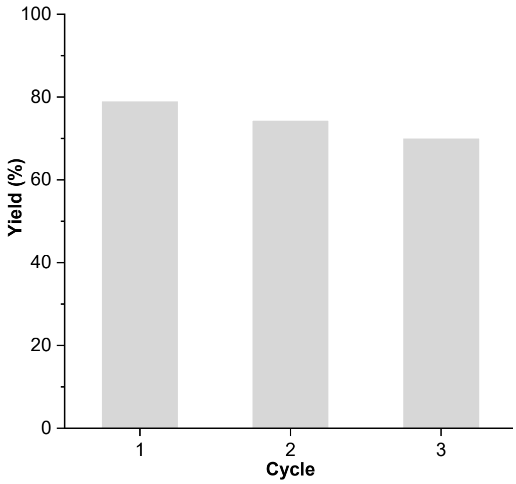

Fig 14. Reusability test for SiO_2-TiO_2/Cu(II). Reaction condition: catalyst, 50 mg; reactants, PhMgBr dan BrPh, 1 mmol for each; solvent, deoxygenated THF, 2 mL; time, 6 h; temperature, 50 °C; and method, stirring heating

which may reduce the number of available active sites, thereby diminishing the catalytic activity for biphenyl production.

Based on the characterization data and catalytic activity tests, we proposed a reaction mechanism for the Kumada cross-coupling catalyzed by SiO_2-TiO_2/Cu(II), as shown in Fig. 16. The Kumada cross-coupling reaction occurring at Cu(II) active site initiated with the addition step (number 1), where halobenzene was bound to Cu(II) then formed a Cu(II)PhX complex. Subsequently, the halide previously attached to Cu(II) was replaced by the phenyl group from the Grignard reagent through the transmetalation step (number 2), resulting in the formation of a Cu(II)Ph_2 complex. The final step was elimination (was 3), where the two phenyl groups previously bonded to Cu(II) detached to form biphenyl.

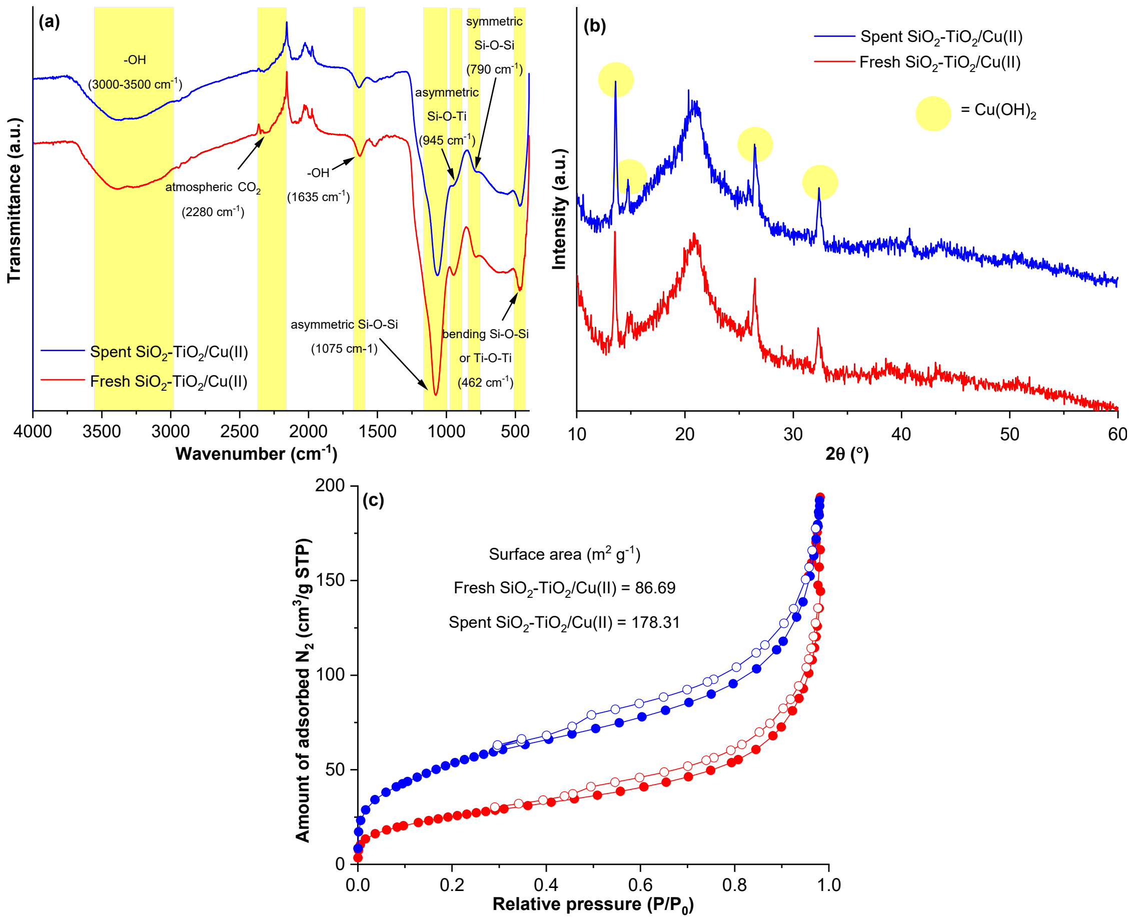

Fig 15. (a) IR spectra, (b) diffraction pattern, and (c) N_2 isotherm adsorption-desorption of fresh (●,○) and spent (●,○) SiO_2-TiO_2/Cu(II). Closed and opened symbols are adsorption and desorption plot, respectively

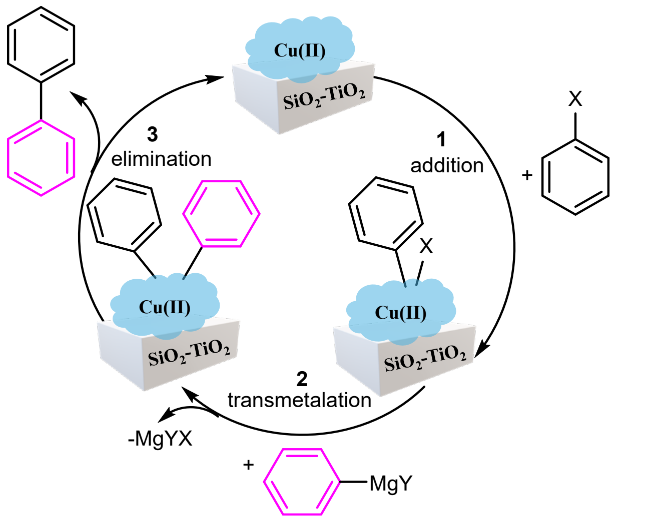

Fig 16. Proposed mechanism of biphenyl synthesis via Kumada cross-coupling reaction catalyzed by SiO_2-TiO_2/Cu(II)

This mechanism continued until all reactant molecules were completely converted. Finally, we isolated the biphenyl compound produced from the Kumada cross-coupling reaction catalyzed by SiO_2-TiO_2/Cu(II) under the optimized conditions. To confirm that the isolated white crystalline solids were biphenyl, characterizations were performed using FTIR, ^{1}H-NMR, ^{13}C-NMR, CHNS analysis, and melting point analysis. Fig. 17(a) shows the IR spectra of the isolated biphenyl compound. The spectra exhibit characteristic vibration corresponding to biphenyl structure including the bands at 3050 cm^{-1} (Csp^2–H stretching), below 2000 cm^{-1} (benzene overtones), 1500–1600 cm^{-1} (C=C aromatic stretching), 1080 cm^{-1} (Csp^2–H in-plane bending), and 720 cm^{-1} (monosubstituted benzene). Fig. 17(b) and 17(c) show the ^{1}H-NMR (500 MHz, chloroform-D) and ^{13}C-NMR (126 MHz, chloroform-D) spectra of the isolated biphenyl, respectively. The ^{1}H-NMR spectra exhibited chemical shifts at δ 7.32–7.35 (m, 2H), 7.41–7.44 (m, 4H), and 7.58–7.59 ppm (m, 4H), while the ^{13}C-NMR showed 4 signals at δ 127.2, 127.2, 128.7, and 141.2 ppm.

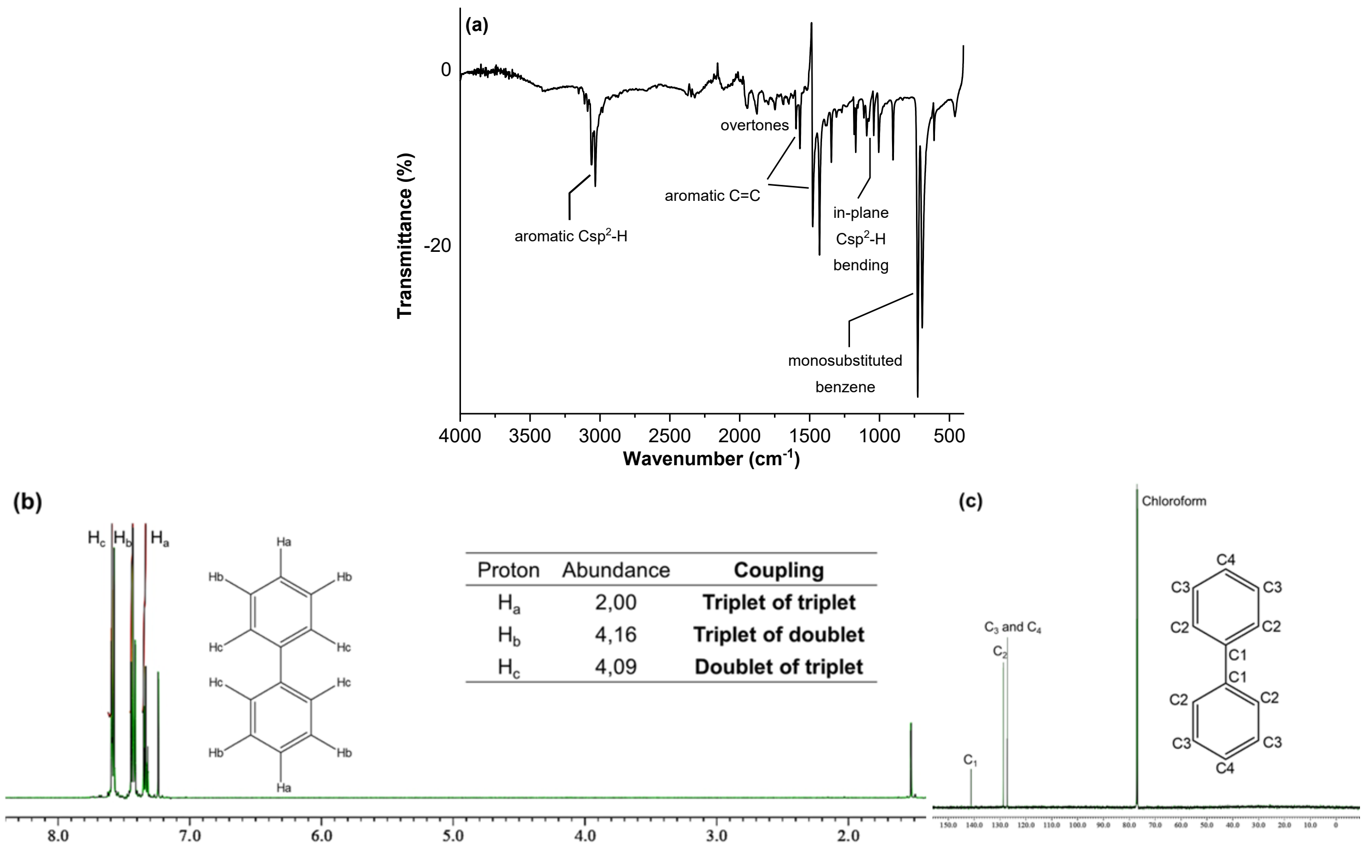

Fig 17. (a) IR, (b) ^{1}H-, and (c) ^{13}C-NMR spectra of the isolated biphenyl

Table 6. CHNS analysis data of the isolated biphenyl (sample mass = 1.993 mg)

Element	Percentage (%)	Mass (mg)	Mol (mmol)
Carbon	93.47	0.00186	0.000155
Hydrogen	6.40	0.00012	0.000127

Mol ratio C/H = 1.217; Empirical formula = $(C_{12}H_{10})_n$; Molecular formula = $C_{12}H_{10}$

Table 7. Melting point analysis data of the isolated biphenyl

Trial	Observed melting point (°C)
1	69
2	70
3	69

These spectra confirm the high purity of the isolated biphenyl, although it still contained a trace amount of water. The purity of the isolated biphenyl was further confirmed by CHNS (Table 6) and melting point analysis (Table 7), which indicate that the isolated biphenyl had a molecular formula of $C_{12}H_{10}$ and an average melting point of 69.3 °C. The molecular formula and average boiling point were found to be consistent with standard biphenyl compound [64].

■ CONCLUSION

In summary, this research showed a novel approach for catalyst preparation by utilizing RHA as the precursor of SiO_2. The extracted SiO_2 was then combined with TiO_2 and the composite was used as support material for Cu(II) immobilization. Through comprehensive material characterization methods, the successful preparation of SiO_2-TiO_2/Cu(II) materials were confirmed, with Cu(II) predominantly existing as $Cu(OH)_2$ on the catalyst surface. The catalyst exhibited remarkable activity in promoting the Kumada cross-coupling reaction, resulting biphenyl yield of 78.85% under optimized conditions. Notably, the catalyst demonstrated excellent reusability over multiple cycles, underscoring its potential for practical applications. The produced biphenyl could be isolated with high purity proven by the results of organic compound characterizations reported in this study.

■ ACKNOWLEDGMENTS

The authors gratefully acknowledge the support provided by the Ministry of Research, Technology, and Higher Education Indonesia (DRTPM Kemdikbudristek), specifically through the PMDSU scholarship and research funding (Grants: 2193/UN1/DITLIT/Dit-Lit/PT.01.03/2023; 018/E5/PG.02.00.PL/2023), as well as the Enhancing International Publication (EIP) - *Peningkatan Kualitas Publikasi Internasional* (PKPI) program 2023 (Grant: 106.7/E4.4/KU/2023).

■ CONFLICT OF INTEREST

The authors affirm that we have no conflicts of interest to disclose.

■ AUTHOR CONTRIBUTIONS

Dewi Agustiningsih contributed to the conceptualization, methodology development, investigation, formal analysis, and the writing of the original draft. Nuryono participated in the conceptualization, supervision, and the review and editing of the manuscript. Sri Juari Santosa was involved in conceptualization, supervision, and manuscript review and editing. Eko Sri Kunarti contributed to the conceptualization, supervision, formal analysis, and the review and editing of the manuscript.

■ REFERENCES

[1] Urquhart, L., 2018, Top drugs and companies by sales in 2017, *Nat. Rev. Drug Discovery*, 17 (4), 232.

[2] Brown, D.G., and Boström, J., 2016, Analysis of past and present synthetic methodologies on medicinal chemistry: Where have all the new reactions gone?, *J. Med. Chem.*, 59 (10), 4443–4458.

[3] Heravi, M.M., Zadsirjan, V., Hajiabbasi, P., and Hamidi, H., 2019, Advances in Kumada–Tamao–Corriu cross-coupling reaction: An update, *Monatsh. Chem.*, 150 (4), 535–591.

[4] Kiss, Á., Hell, Z., and Bálint, M., 2010, Nickel/magnesium-lanthanum mixed oxide catalyst in the Kumada-coupling, *Org. Biomol. Chem.*, 8 (2), 331–335.

[5] Kiss, Á., Németh, J., Fodor, A., and Hell, Z., 2015, Supported metal catalysts in organic syntheses, *Period. Polytech., Chem. Eng.*, 59 (1), 72–81.

[6] Vásquez-Céspedes, S., Betori, R.C., Cismesia, M.A., Kirsch, J.K., and Yang, Q., 2021, Heterogeneous

catalysis for cross-coupling reactions: An underutilized powerful and sustainable tool in the fine chemical industry?, *Org. Process Res. Dev.*, 25 (4), 740–753.
[7] Ramesh, A., Da, C.T., Manigandan, R., Bhargav, P.B., and Nguyen-Le, M.T., 2022, Selectivity oxidation of benzyl alcohol using mesoporous g-C_3N_4 catalysts prepared by hard template method, *Colloids Interface Sci. Commun.*, 48, 100608.
[8] Zhang, Y.F., and Shi, Z.J., 2019, Upgrading cross-coupling reactions for biaryl syntheses, *Acc. Chem. Res.*, 52 (1), 161–169.
[9] Beletskaya, I.P., and Cheprakov, A.V., 2004, Copper in cross-coupling reactions: The post-Ullmann chemistry, *Coord. Chem. Rev.*, 248 (21), 2337–2364.
[10] Kadu, B.S., 2021, Suzuki-Miyaura cross coupling reaction: Recent advancements in catalysis and organic synthesis, *Catal. Sci. Technol.*, 11 (4), 1186–1221.
[11] Ghorbani-Choghamarani, A., Derakhshan, A.A., Hajjami, M., and Rajabi, L., 2016, Copper-Schiff base alumoxane: A new and reusable mesoporous nano catalyst for Suzuki-Miyaura and Stille C-C cross-coupling reactions, *RSC Adv.*, 6 (97), 94314–94324.
[12] Ali, M.E., Rahman, M.M., Sarkar, S.M., and Abd Hamid, S.B., 2014, Heterogeneous metal catalysts for oxidation reactions, *J. Nanomater.*, 2024 (1), 192038.
[13] Deshmukh, P., Bhatt, J., Peshwe, D., and Pathak, S., 2012, Determination of silica activity index and XRD, SEM and EDS studies of amorphous SiO_2 extracted from rice husk ash, *Trans. Indian Inst. Met.*, 65 (1), 63–70.
[14] Setyawan, N., Hoerudin, H., and Yuliani, S., 2021, Synthesis of silica from rice husk by sol-gel method, *IOP Conf. Ser.: Earth Environ. Sci.*, 733 (1), 012149.
[15] Yuvakkumar, R., Elango, V., Rajendran, V., and Kannan, N., 2014, High-purity nano silica powder from rice husk using a simple chemical method, *J. Exp. Nanosci.*, 9 (3), 272–281.
[16] Nayak, P.P., and Datta, A.K., 2021, Synthesis of SiO_2-nanoparticles from rice husk ash and its comparison with commercial amorphous silica through material characterization, *Silicon*, 13 (4), 1209–1214.
[17] Mejía, J.M., Mejía de Gutiérrez, R., and Montes, C., 2016, Rice husk ash and spent diatomaceous earth as a source of silica to fabricate a geopolymeric binary binder, *J. Cleaner Prod.*, 118, 133–139.
[18] Bagheri, S., Muhd Julkapli, N., and Bee Abd Hamid, S., 2014, Titanium dioxide as a catalyst support in heterogeneous catalysis, *Sci. World J.*, 2014 (1), 727496.
[19] Palcheva, R., Dimitrov, L., Tyuliev, G., Spojakina, A., and Jiratova, K., 2013, TiO_2 nanotubes supported NiW hydrodesulphurization catalysts: Characterization and activity, *Appl. Surf. Sci.*, 265, 309–316.
[20] Ulfa, M., Al Afif, H., Saraswati, T.E., and Bahruji, H., 2022, Fast removal of methylene blue via adsorption-photodegradation on TiO_2/SBA-15 synthesized by slow calcination, *Materials*, 15 (16), 5471.
[21] Agustiningsih, D., Otomo, R., Kamiya, Y., Nuryono, N., Santosa, S.J., and Kunarti, E.S., 2024, Fixing Ni^{2+} onto mesoporous SiO_2-TiO_2 through amino silane and application as a catalyst for Kumada cross coupling reaction for 1,1'-biphenyl synthesis, *Appl. Catal., A*, 672, 119606.
[22] Agustiningsih, D., Kunarti, E.S., Nuryono, N., Santosa, S.J., Mardjan, M.I.D., Kamiya, Y., and Otomo, R., 2024, Novel nickel-immobilized-SiO_2-TiO_2 fine particles in the presence of cetyltrimethylammonium bromide as a catalyst for ultrasound-assisted-Kumada cross-coupling reaction, *Heliyon*, 10 (14), e34614.
[23] Kiani, F., and Naeimi, H., 2018, Ultrasonic accelerated coupling reaction using magnetically recyclable bis (propyl molononitril) Ni complex nanocatalyst: A novel, green and efficient synthesis of biphenyl derivatives, *Ultrason. Sonochem.*, 48, 267–274.
[24] Esmaeilpour, M., Zahmatkesh, S., Fahimi, N., and Nosratabadi, M., 2018, Palladium nanoparticles immobilized on EDTA-modified Fe_3O_4@SiO_2 nanospheres as an efficient and magnetically separable catalyst for Suzuki and Sonogashira cross-coupling reactions, *Appl. Organomet. Chem.*, 32 (4), e4302.
[25] Akkoç, M., Buğday, N., Altın, S., Kiraz, N., Yaşar, S.,

and Özdemir, İ., 2021, *N*-heterocyclic carbene Pd(II) complex supported on Fe_3O_4@SiO_2: Highly active, reusable and magnetically separable catalyst for Suzuki-Miyaura cross-coupling reactions in aqueous media, *J. Organomet. Chem.*, 943, 121823.

[26] Fan, X., Yang, J., Pang, Q., Liu, Z., Zhang, P., and Yang, J.H., 2021, Ultrafine and highly dispersed Pd/SiO_2 for Suzuki–Miyaura cross-coupling reactions, *Catal. Lett.*, 151 (8), 2291–2301.

[27] Khandaka, H., Sharma, K.N., and Joshi, R.K., 2021, Aerobic Cu and amine free Sonogashira and Stille couplings of aryl bromides/chlorides with a magnetically recoverable Fe_3O_4@SiO_2 immobilized Pd(II)-thioether containing NHC, *Tetrahedron Lett.*, 67, 152844.

[28] Eslahi, H., Sardarian, A.R., and Esmaeilpour, M., 2021, Green and sustainable palladium nanomagnetic catalyst stabilized by glucosamine-functionalized Fe_3O_4@SiO_2 nanoparticles for Suzuki and Heck reactions, *Appl. Organomet. Chem.*, 35 (7), e6260.

[29] Zhao, Y., Huang, Z., Wang, L., Chen, X., Zhang, Y., Yang, X., Pang, D., Kang, J., and Guo, L., 2022, Highly efficient and recyclable amorphous Pd(II)/crystal Pd(0) catalyst for boosting Suzuki reaction in aqueous solution, *Nano Res.*, 15 (2), 1193–1198.

[30] Ghabdian, K., Motavalizadehkakhky, A., Zhiani, R., Heravi, M.M., Allahresani, A., and Zadsirjan, V., 2023, (Fe_3O_4@SiO_2/GO–NH_2–CoII NPs): A novel and efficient nanomagnetic heterogeneous cobalt catalysis in the Sonogashira and Heck–Mizoroki coupling reactions, *J. Cluster Sci.*, 34 (6), 3105–3119.

[31] Nasseri, F., Nasseri, M.A., Kassaee, M.Z., and Yavari, I., 2023, Synergistic performance of a new bimetallic complex supported on magnetic nanoparticles for Sonogashira and C–N coupling reactions, *Sci. Rep.*, 13 (1), 18153.

[32] Abdalrazaq, E.A., Mohammed, H.K., Voronkova, D.K., Joshi, S.K., Saleh, E.A.M., Kareem, A.H., Kumar, A., Alawadi, A., Alslaami, A., and Fathollahi, R., 2024, Palladium anchored to BisPyP@bilayer-SiO_2@NMP organic–inorganic hybrid as an efficient and recoverable novel nanocatalyst in Suzuki and Stille C–C coupling reactions, *Sci. Rep.*, 14 (1), 8945.

[33] Sharma, H., Mahajan, H., Jamwal, B., and Paul, S., 2018, Cu@Fe_3O_4-TiO_2-L-dopa: A novel and magnetic catalyst for the Chan-Lam cross-coupling reaction in ligand free conditions, *Catal. Commun.*, 107, 68–73.

[34] Eskandari, A., Jafarpour, M., Rezaeifard, A., and Salimi, M., 2019, Supramolecular photocatalyst of palladium (II) encapsulated within Dendrimer on TiO_2 nanoparticles for photo-induced Suzuki-Miyaura and Sonogashira cross-coupling reactions, *Appl. Organomet. Chem.*, 33 (10), e5093.

[35] Feizpour, F., Jafarpour, M., and Rezaeifard, A., 2019, Band gap modification of TiO_2 nanoparticles by ascorbic acid-stabilized Pd nanoparticles for photocatalytic Suzuki–Miyaura and Ullmann coupling reactions, *Catal. Lett.*, 149 (6), 1595–1610.

[36] Chen, Y., and Feng, L., 2020, Silver nanoparticles doped TiO_2 catalyzed Suzuki-coupling of bromoaryl with phenylboronic acid under visible light, *J. Photochem. Photobiol., B*, 205, 111807.

[37] Adam, M.S.S., Ullah, F., and Makhlouf, M.M., 2020, Hybrid organic-inorganic Cu(II) iminoisonicotine@TiO_2@Fe_3O_4 heterostructure as efficient catalyst for cross-couplings, *J. Am. Ceram. Soc.*, 103 (8), 4632–4653.

[38] Banda, P.G., and Mucherla, R., 2022, Palladium-supported polydopamine-coated $NiFe_2O_4$@TiO_2: A sole photocatalyst for Suzuki and Sonogashira coupling reactions under sunlight irradiation, *ACS Omega*, 7 (33), 29356–29368.

[39] Hosseini-Sarvari, M., and Dehghani, A., 2023, Nickel/TiO_2-catalyzed Suzuki–Miyaura cross-coupling of arylboronic acids with aryl halides in MeOH/H_2O, *Monatsh. Chem.*, 154 (3), 397–405.

[40] Gandra, U.R., Reddy, P.S., Salam, A., Gajagouni, S.P., Alfantazi, A., and Mohideen, M.I.H., 2024, TiO_2 supported pallidum-bipyridyl complex as an efficient catalyst for Suzuki–Miyaura reaction in aqueous-ethanol, *Sci. Rep.*, 14 (1), 7323.

[41] Wu, Y., Zhang, Y., Zhou, J., and Gu, D., 2020, Recent

progress on functional mesoporous materials as catalysts in organic synthesis, *Emergent Mater.*, 3 (3), 247–266.

[42] Piyathissa, S.D.S., Kahandage, P.D., Namgay, N., Zhang, H., Noguchi, R., and Ahamed, T., 2023, Introducing a novel rice husk combustion technology for maximizing energy and amorphous silica production environmental impacts and health risk, *Energies*, 16 (3), 1120.

[43] Yan, S., Yin, D., He, F., Cai, J., Schliermann, T., and Behrendt, F., 2022, Characteristics of smoldering on moist rice husk for silica production, *Sustainability*, 14 (1), 317.

[44] Ajeel, S.A., Sukkar, K.A., and Zedin, N.K., 2020, Extraction of high purity amorphous silica from rice husk by chemical process, *IOP Conf. Ser.: Mater. Sci. Eng.*, 881 (1), 012096.

[45] Askaruly, K., Azat, S., Sartova, Z., Yeleuov, M., Kerimkulova, A., and Bekseitova, K., 2020, Obtaining and characterization of amorphous silica from rice husk, *J. Chem. Technol. Metall.*, 55 (1), 88–97.

[46] Aharipour, N., Nemati, A., and Malek Khachatourian, A., 2022, Green synthesis of silica extracted from rice husk ash, *Adv. Ceram. Prog.*, 8 (4), 15–20.

[47] Sawasdee, V., and Pisutpaisal, N., 2022, Rice husk ash characterization and utilization as a source of silica material, *Chem. Eng. Trans.*, 93, 79–84.

[48] Carvalho, G.C., Marena, G.D., Karnopp, J.C.F., Jorge, J., Sábio, R.M., Martines, M.A.U., Bauab, T.M., and Chorilli, M., 2022, Cetyltrimethylammonium bromide in the synthesis of mesoporous silica nanoparticles: General aspects and *in vitro* toxicity, *Adv. Colloid Interface Sci.*, 307, 102746.

[49] Nurhadi, M., 2017, Modification of coal char-loaded TiO_2 by sulfonation and alkylsilylation to enhance catalytic activity in styrene oxidation with hydrogen peroxide as oxidant, *Bull. Chem. React. Eng. Catal.*, 12 (1), 55–61.

[50] Hikmah, N., Agustiningsih, D., Nuryono, N., and Kunarti, E.S., 2022, Preparation of iron-doped SiO_2/TiO_2 using silica from sugarcane bagasse ash for visible light degradation of Congo red, *Indones. J. Chem.*, 22 (2), 402–412.

[51] Rizal, U., Das, S., Kumar, D., Swain, B.S., and Swain, B.P., 2016, Synthesis and characterization of TiO_2 nanostructure thin films grown by thermal CVD, *AIP Conf. Proc.*, 1724 (1), 020115.

[52] Bakri, A.S., Sahdan, M.Z., Adriyanto, F., Raship, N.A., Said, N.D.M., Abdullah, S.A., and Rahim, M.S., 2017, Effect of annealing temperature of titanium dioxide thin films on structural and electrical properties, *AIP Conf. Proc.*, 1788 (1), 030030.

[53] Malevu, T.D., Mwankemwa, B.S., Motloung, S.V., Tshabalala, K.G., and Ocaya, R.O., 2019, Effect of annealing temperature on nano-crystalline TiO_2 for solar cell applications, *Phys. E*, 106, 127–132.

[54] Akrami, S., Watanabe, M., Ling, T.H., Ishihara, T., Arita, M., Fuji, M., and Edalati, K., 2021, High-pressure TiO_2-II polymorph as an active photocatalyst for CO_2 to CO conversion, *Appl. Catal., B*, 298, 120566.

[55] Agustiningsih, D., Nuryono, N., Santosa, S.J., and Kunarti, E.S., 2023, Propylamine silica-titania hybrid material modified with Ni(II) as the catalyst for benzyl alcohol to benzaldehyde conversion, *Indones. J. Chem.*, 23 (5), 1361–1374.

[56] Wang, L., Zhang, K., Hu, Z., Duan, W., Cheng, F., and Chen, J., 2014, Porous CuO nanowires as the anode of rechargeable Na-ion batteries, *Nano Res.*, 7 (2), 199–208.

[57] Zimbovskiy, D.S., Gavrilov, A.I., and Churagulov, B.R., 2018, Synthesis of copper oxides films via anodic oxidation of copper foil followed by thermal reduction, *IOP Conf. Ser.: Mater. Sci. Eng.*, 347 (1), 012010.

[58] Wang, J., Ran, Q., Xu, X., Zhu, B., and Zhang, W., 2019, Preparation and optical properties of TiO_2-SiO_2 thin films by sol-gel dipping method, *IOP Conf. Ser.: Earth Environ. Sci.*, 310 (4), 042029.

[59] Kocjan, A., Logar, M., and Shen, Z., 2017, The agglomeration, coalescence and sliding of nanoparticles, leading to the rapid sintering of zirconia nanoceramics, *Sci. Rep.*, 7 (1), 2541.

[60] Tian, Y., Jiao, W., Liu, P., Song, S., Lu, Z., Hirata, A., and Chen, M., 2019, Fast coalescence of metallic glass nanoparticles, *Nat. Commun.*, 10 (1), 5249.

[61] Busacca, C.A., Fandrick, D.R., Song, J.J., and Senanayake, C.H., 2012, "Transition Metal Catalysis in the Pharmaceutical Industry" in *Applications of Transition Metal Catalysis in Drug Discovery and Development*, John Wiley & Sons, Inc., Hoboken, New Jersey, US, 1–24.

[62] Mondal, P., Bhanja, P., Khatun, R., Bhaumik, A., Das, D., and Manirul Islam, S., 2017, Palladium nanoparticles embedded on mesoporous TiO_2 material (Pd@$MTiO_2$) as an efficient heterogeneous catalyst for Suzuki-Coupling reactions in water medium, *J. Colloid Interface Sci.*, 508, 378–386.

[63] Sancheti, S.V., and Gogate, P.R., 2018, Intensification of heterogeneously catalyzed Suzuki-Miyaura cross-coupling reaction using ultrasound: Understanding effect of operating parameters, *Ultrason. Sonochem.*, 40, 30–39.

[64] U.S. Environmental Protection Agency, 2010, *Toxicological Review of Biphenyl*, EPA/635/R-11/005F, https://iris.epa.gov/static/pdfs/0013tr.pdf.